JACS
JOURNAL OF THE AMERICAN CHEMICAL SOCIETY

Article

Molecular Dynamics Simulation of Amphiphilic Bistable [2]Rotaxane Langmuir Monolayers at the Air/Water Interface

Seung Soon Jang, Yun Hee Jang, Yong-Hoon Kim, William A. Goddard, Jang Wook Choi, James R. Heath, Bo W. Laursen, Amar H. Flood, J. Fraser Stoddart, Kasper Nrgaard, and Thomas Bjrnholm

J. Am. Chem. Soc., **2005**, 127 (42), 14804-14816• DOI: 10.1021/ja0531531 • Publication Date (Web): 27 September 2005

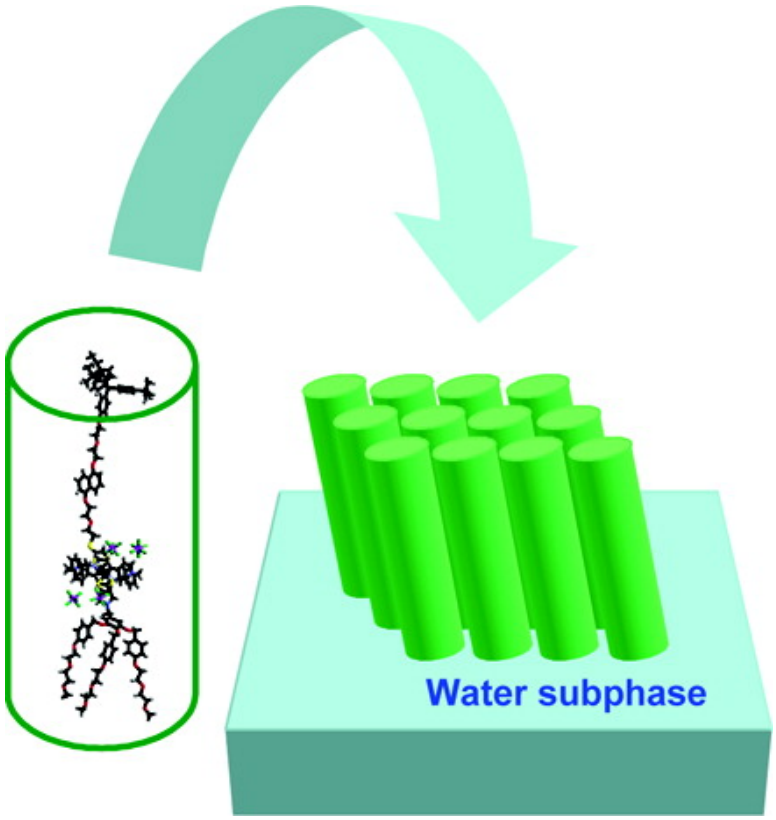

More About This Article

Additional resources and features associated with this article are available within the HTML version:

- Supporting Information
- Links to the 14 articles that cite this article, as of the time of this article download
- Access to high resolution figures

Journal of the American Chemical Society is published by the American Chemical Society. 1155 Sixteenth Street N.W., Washington, DC 20036

J|A|C|S
ARTICLES
Published on Web 09/27/2005

Molecular Dynamics Simulation of Amphiphilic Bistable [2]Rotaxane Langmuir Monolayers at the Air/Water Interface

Seung Soon Jang,[†] Yun Hee Jang,[†] Yong-Hoon Kim,[†,#] William A. Goddard III,*[,†] Jang Wook Choi,[‡] James R. Heath,[‡] Bo W. Laursen,[§,⊥] Amar H. Flood,[§] J. Fraser Stoddart,[§] Kasper Nørgaard,[⊥] and Thomas Bjørnholm[⊥]

Contribution from the Materials and Process Simulation Center (139-74) and Division of Chemistry and Chemical Engineering (127-72), California Institute of Technology, Pasadena, California 91125, California NanoSystems Institute and Department of Chemistry and Biochemistry, University of California, Los Angeles, 405 Hilgard Avenue, Los Angeles, California 90095-1569, and Nano-Science Center and Department of Chemistry, University of Copenhagen, Universitetsparken 5, DK-2100 København Ø, Denmark

Received May 13, 2005; E-mail: wag@wag.caltech.edu

Abstract: Bistable [2]rotaxanes display controllable switching properties in solution, on surfaces, and in devices. These phenomena are based on the electrochemically and electrically driven mechanical shuttling motion of the ring-shaped component, cyclobis(paraquat-*p*-phenylene) ($CBPQT^{4+}$), between a monopyrrolotetrathiafulvalene (mpTTF) unit and a 1,5-dioxynaphthalene (DNP) unit located along a dumbbell component. The most stable state of the rotaxane ($CBPQT^{4+}$@mpTTF) is that in which the $CBPQT^{4+}$ ring encircles the mpTTF unit, but a second less favored metastable co-conformation with the $CBPQT^{4+}$ ring surrounding the DNP ($CBPQT^{4+}$@DNP) can be formed experimentally. For both co-conformations of an amphiphilic bistable [2]rotaxane, we report here the structure and surface pressure−area isotherm of a Langmuir monolayer (LM) on a water subphase as a function of the area per molecule. These results from atomistic molecular dynamics (MD) studies are validated by comparing with experiments based on similar amphiphilic rotaxanes. For both co-conformations, we found that as the area per molecule increases the thickness of the LM decreases while the molecular tilt increases. Both co-conformations led to similar LM thicknesses at the same packing area. From the simulated LM systems, we calculated the electron density profiles of the monolayer as a function of area per molecule, which show good agreement with experimental analyses from synchrotron X-ray reflectivity measurements of related systems. Decomposing the overall electron density profiles into component contributions, we found distinct differences in molecular packing in the film depending upon the co-conformation. Thus we find that the necessity of allowing the tetracationic ring to become solvated by water leads to differences in the structures for the two co-conformations in the LM. At the same packing area, the value of the overall tilt angle does not seem to be sensitive to whether the $CBPQT^{4+}$ ring is encircling the mpTTF or the DNP unit. However, the conformation of the dumbbell does depend on the location of the $CBPQT^{4+}$ ring, which is reflected in the segmental tilt angles of the mpTTF and DNP units. Using the Kirkwood−Buff formula in conjunction with MD calculations, we find the surface pressure−area isotherms for each co-conformation in which the $CBPQT^{4+}$@mpTTF form has smaller surface tension and therefore larger surface pressure than the $CBPQT^{4+}$@DNP at the same packing area, differences that decreases with increasing area per molecule, which is verified experimentally.

1. Introduction

Functional nanoscale devices based on molecular machines[1−7] are being developed experimentally for applications ranging from nanoelectronics[8−10] to nanomechanics.[1−7,10−12] Particularly interesting are the bistable [2]rotaxanes[13] (Figure 1), which enable controlled linear motions.[14−18] We will focus on the

[†] Materials and Process Simulation Center, California Institute of Technology.
[‡] Division of Chemistry and Chemical Engineering, California Institute of Technology.
[§] University of California, Los Angeles.
[⊥] University of Copenhagen.
[#] Current address: Korea Institute for Advanced Study, 207-43 Cheongnyangni 2-dong, Dongdaemun-gu, Seoul 130-722, Korea.

(1) Barboiu, M.; Lehn, J.-M. *Proc. Natl. Acad. Sci. U.S.A.* **2002**, *99*, 5201−5206.
(2) Hogg, L.; Leigh, D. A.; Lusby, P. J.; Morelli, A.; Parsons, S.; Wong, J. K. Y. *Angew. Chem., Int. Ed.* **2004**, *43*, 1218−1221.
(3) Zheng, X.; Mulcahy, M. E.; Horinek, D.; Galeotti, F.; Magnera, T. F.; Michl, J. *J. Am. Chem. Soc.* **2004**, *126*, 4540−4542.
(4) Hawthorne, M. F.; Zink, J. I.; Skelton, J. M.; Bayer, M. J.; Liu, C.; Livshits, E.; Baer, R.; Neuhauser, D. *Science* **2004**, *303*, 1849−1851.
(5) de Jong, J. J. D.; Lucas, L. N.; Kellogg, R. M.; van Esch, J. H.; Reringa, B. L. *Science* **2004**, *304*, 278−281.
(6) Turberfield, A. J.; Mitchell, J. C.; Yurke, B.; Mills, A. P.; Blakey, M. I.; Simmel, F. C. *Phys. Rev. Lett.* **2003**, *90*, 118102.
(7) Liu, H. Q.; Schmidt, J. J.; Bachand, G. D.; Rizk, S. S.; Looger, L. L.; Hellinga, H. W.; Montemagno, C. D. *Nat. Mater.* **2002**, *1*, 173−177.
(8) Reed, M. A., Lee, T., Eds. *Molecular Nanoelectronics*; American Scientific Publishers: Stevenson Ranch, 2003.
(9) Flood, A. H.; Ramirez, R. J. A.; Deng, W.-Q.; Muller, R. P.; Goddard, W. A., III; Stoddart, J. F. *Aust. J. Chem.* **2004**, *57*, 301−322.
(10) Balzani, V.; Credi, A.; Venturi, M. *Molecular Devices and Machines—A Journey into the Nano World*; Wiley-VCH: Weinheim, 2003.
(11) Hanke, A.; Metzler, R. *Chem. Phys. Lett.* **2002**, *359*, 22−26.

10.1021/ja0531531 CCC: $30.25

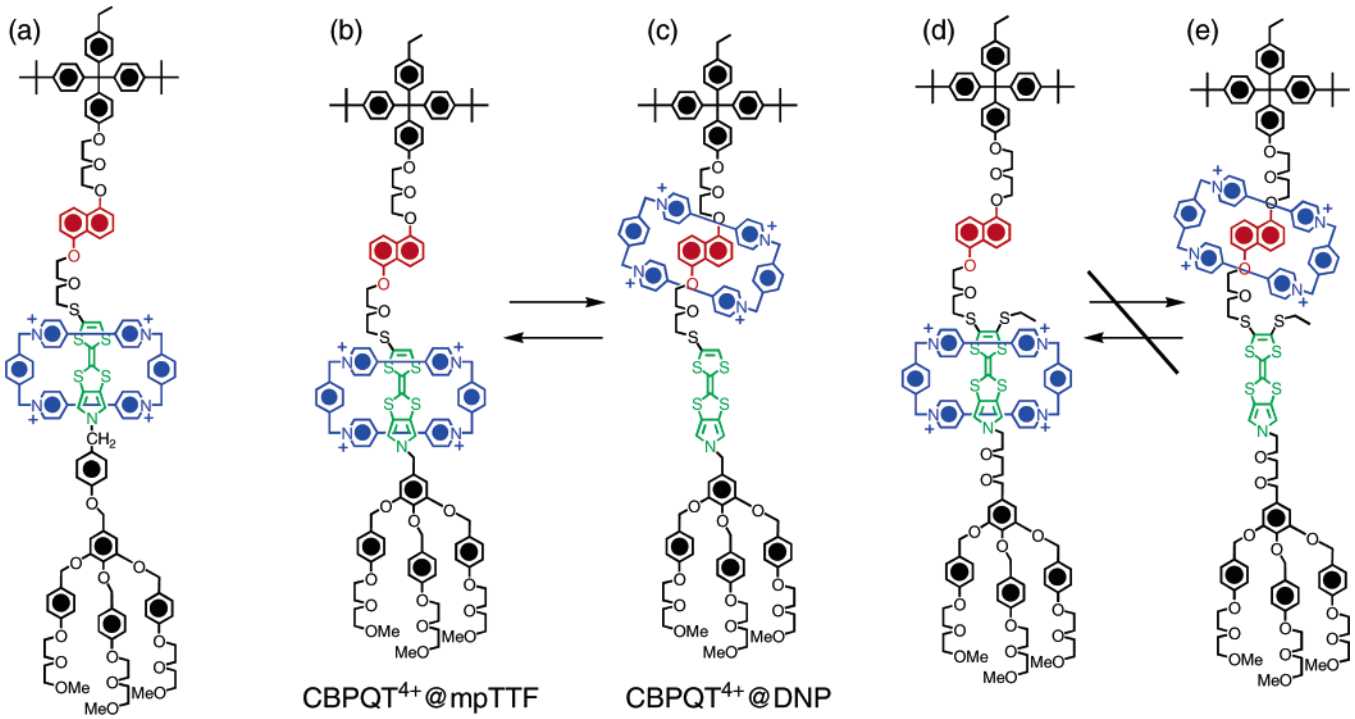

Figure 1. Structural formulas of the amphiphilic bistable [2]rotaxanes (a) used experimentally and modeled in this study in the (b) $CBPQT^{4+}$@mpTTF co-conformation and the (c) $CBPQT^{4+}$@DNP co-conformation, as well as of the blocked amphiphilic [2]rotaxanes used in the X-ray reflectivity experiments and as model compounds for each co-conformation: (d) blocked $CBPQT^{4+}$@mpTTF and (e) blocked $CBPQT^{4+}$@DNP. Shuttling movement of the $CBPQT^{4+}$ ring in the blocked rotaxanes is prevented on account of the additional ethyl group on the mpTTF station.

redox-controllable [2]rotaxanes composed of (1) an electron-accepting cyclobis(paraquat-*p*-phenylene) ($CBPQT^{4+}$) ring that can be induced to shuttle between two electron-donating stations, which we consider as (2) a monopyrrolotetrathiafulvalene (mpTTF) unit and (3) a 1,5-dioxynaphthalene (DNP) unit. The energetically favored ground state of the rotaxane has the $CBPQT^{4+}$ ring encircling the mpTTF unit ($CBPQT^{4+}$@mpTTF co-conformation), whereas the less favored metastable state displays the $CBPQT^{4+}$ ring on the DNP unit ($CBPQT^{4+}$@DNP co-conformation). The salient feature of bistable rotaxanes is that the co-conformation can be switched[9,16−20] between the mpTTF and DNP units by electrochemical means, thereby inducing controlled nanometer-scale movements. Bistable [2]-rotaxanes modified to be amphiphilic[12,13,19,21−25] have been incorporated[9,13,19] as close-packed monolayers between two-terminal electronic memory devices. These devices display OFF−ON switching behavior between low and high currents. The former state is stable at room temperature, whereas the latter is only metastable,[13,18,26] and these two states are proposed to be associated with the location of the $CBPQT^{4+}$ ring.[9,13,27] Accordingly, the $CBPQT^{4+}$@mpTTF co-conformation is hypothesized[13,18] to have a low conductance and is thus assigned to the OFF state of the electronic devices. The ON state, which displays a conductance 3−10 times larger, is assigned to the $CBPQT^{4+}$@DNP co-conformation. These and other novel features of bistable [2]rotaxanes[21−25] and bistable [2]catenanes[16−18] lay the foundation for many new types of molecular-level devices, with significant efforts focusing on the generic switching behavior of molecular switches[16,17,19,20,28−33] and molecular

(12) Tseng, H. R.; Vignon, S. A.; Stoddart, J. F. *Angew. Chem., Int. Ed.* **2003**, *42*, 1491−1495.
(13) Luo, Y.; Collier, C. P.; Jeppesen, J. O.; Nielsen, K. A.; Delonno, E.; Ho, G.; Perkins, J.; Tseng, H. R.; Yamamoto, T.; Stoddart, J. F.; Heath, J. R. *ChemPhysChem* **2002**, *3*, 519−525.
(14) Anelli, P. L.; Spencer, N.; Stoddart, J. F. *J. Am. Chem. Soc.* **1991**, *113*, 5131−5133.
(15) Bissell, R. A.; Cordova, E.; Kaifer, A. E.; Stoddart, J. F. *Nature* **1994**, *369*, 133−137.
(16) Asakawa, M.; Ashton, P. R.; Balzani, V.; Credi, A.; Hamers, C.; Mattersteig, G.; Montalti, M.; Shipway, A. N.; Spencer, N.; Stoddart, J. F.; Tolley, M. S.; Venturi, M.; White, A. J. P.; Williams, D. J. *Angew. Chem., Int. Ed.* **1998**, *37*, 333−337.
(17) Balzani, V.; Credi, A.; Mattersteig, G.; Matthews, O. A.; Raymo, F. M.; Stoddart, J. F.; Venturi, M.; White, A. J. P.; Williams, D. J. *J. Org. Chem.* **2000**, *65*, 1924−1936.
(18) Collier, C. P.; Mattersteig, G.; Wong, E. W.; Luo, Y.; Beverly, K.; Sampaio, J.; Raymo, F. M.; Stoddart, J. F.; Heath, J. R. *Science* **2000**, *289*, 1172−1175.
(19) Collier, C. P.; Jeppesen, J. O.; Luo, Y.; Perkins, J.; Wong, E. W.; Heath, J. R.; Stoddart, J. F. *J. Am. Chem. Soc.* **2001**, *123*, 12632−12641.
(20) Diehl, M. R.; Steuerman, D. W.; Tseng, H. R.; Vignon, S. A.; Star, A.; Celestre, P. C.; Stoddart, J. F.; Heath, J. R. *ChemPhysChem.* **2003**, *4*, 1335−1339.
(21) Jeppesen, J. O.; Perkins, J.; Becher, J.; Stoddart, J. F. *Angew. Chem., Int. Ed.* **2001**, *40*, 1216−1221.
(22) Jeppesen, J. O.; Nielsen, K. A.; Perkins, J.; Vignon, S. A.; Di Fabio, A.; Ballardini, R.; Gandolfi, M. T.; Venturi, M.; Balzani, V.; Becher, J.; Stoddart, J. F. *Chem. Eur. J.* **2003**, *9*, 2982−3007.
(23) Yamamoto, T.; Tseng, H. R.; Stoddart, J. F.; Balzani, V.; Credi, A.; Marchioni, F.; Venturi, M. *Collect. Czech. Chem. Commun.* **2003**, *68*, 1488−1514.
(24) Huang, T. J.; Tseng, H.-R.; Sha, L.; Lu, W.; Brough, B.; Flood, A. H.; Yu, B.-D.; Celestre, P. C.; Chang, J. P.; Stoddart, J. F.; Ho, C.-M. *Nano Lett.* **2004**, *4*, 2065−2071.
(25) Kang, S. S.; Vignon, S. A.; Tseng, H. R.; Stoddart, J. F. *Chem. Eur. J.* **2004**, *10*, 2555−2564.
(26) Flood, A. H.; Stoddart, J. F.; Steuerman, D. W.; Heath, J. R. *Science* **2004**, *306*, 2055−2056.
(27) Kim, Y.-H.; Jang, S. S.; Jang, Y. H.; Goddard, W. A., III. *Phys. Rev. Lett.* **2005**, *94*, 156801.
(28) Credi, A.; Balzani, V.; Langford, S. J.; Stoddart, J. F. *J. Am. Chem. Soc.* **1997**, *119*, 2679−2681.
(29) Collier, C. P.; Wong, E. W.; Belohradsky, M.; Raymo, F. M.; Stoddart, J. F.; Kuekes, P. J.; Williams, R. S.; Heath, J. R. *Science* **1999**, *285*, 391−394.
(30) Elizarov, A. M.; Chiu, S. H.; Stoddart, J. F. *J. Org. Chem.* **2002**, *67*, 9175−9181.
(31) Carroll, R. L.; Gorman, C. B. *Angew. Chem., Int. Ed.* **2002**, *41*, 4379−4400.
(32) Yu, H. B.; Luo, Y.; Beverly, K.; Stoddart, J. F.; Tseng, H. R.; Heath, J. R. *Angew. Chem., Int. Ed.* **2003**, *42*, 5706−5711.

machines[34−39] from solution,[12,16,17,21−23,25,40−42] embedded in polymer electrolyte gels,[43] onto surfaces,[44−46] and incorporated[18−20] into devices.

To develop nanoscale devices based on such synthetic molecular machines, it is essential to incorporate them reliably into integrated solid-state and "wet" devices.[47−51] One promising mode of integration is supramolecular self-organization,[52−59] harnessing interfacial, intermolecular dynamic noncovalent (and sometimes covalent) bonding interactions to form self-assembled monolayers (SAMs)[38,45,46,60−63] and Langmuir−Blodgett (LB)[44,64−67] films on various surfaces. Such self-organized structures offer a range of benefits, and practical methods for manipulating SAMs and LB films of various organic molecules are well-established.[68]

To design any reliable devices based on such complex molecules, it is essential to have a detailed knowledge of the self-organized superstructures of amphiphilic bistable rotaxanes within monolayers and how this affects the fundamental nanoelectromechanical behavior of these rotaxanes. This would allow the molecular architecture and its packing in a device to be optimized to improve its performance. Unfortunately, it is difficult to obtain from experiment such atomistic level characterization of the conformation of each molecule within the self-organized supramolecular structures. Even so, studies on the self-assembly of rotaxanes[19,38,45,60−67] are beginning to give valuable experimental information about the conformations,[25,44] co-conformations,[66] and mechanical movements[18,45,66] within the monolayers.

To provide such atomistic level information, we have been developing first-principles methods to predict conformational and structural parameters of films of rotaxanes and catenanes and the properties (redox potentials, conductances, vibrational frequencies, binding energies, surface tensions) associated with such films as a function of the architecture. We expect that this will play a vital role for rationalizing experimental results and as a foundation for computer-guided design of next-generation molecular switches and nanoscale devices.[69] The advantage of the simulations is that we obtain details of the structures and properties and how they depend on architecture. The disadvantage is not knowing how the experimental techniques of synthesizing the films might bias the results. Thus it is most valuable to find systems for which there can be such a direct comparison, at least for a few properties. In this paper we have chosen to model and simulate Langmuir monolayers (LMs) since the experimental structures can be controlled, increasing the chance that the simulations would be on the same structures as the experiments. Again, the experiments do not lead to atomistic level information, but the pressure as a function of area per molecule can be measured and calculated, as can the vertical density distribution from grazing incidence X-ray diffraction and reflection experiments. In addition, the surface tension of the films can be measured. All three of these properties can be measured for both the ON and OFF states.

In this paper, we use fully atomistic molecular dynamics (MD) simulations at 300 K to predict the structures and properties for LMs of the amphiphilic bistable [2]rotaxanes obtained (Figure 1b,c). Here we consider amphiphilic bistable rotaxanes that are simplifications of two different amphiphilic rotaxanes. One rotaxane is bistable and studied using X-ray reflectivity studies[68] (Figure 1a) to obtain the electron density distribution perpendicular to the LM. In addition, we consider two blocked rotaxanes synthetically prepared in their $CBPQT^{4+}$@mpTTF and $CBPQT^{4+}$@DNP forms in LMs (Figure 1d,e).

2. Simulation Details

2.1. Force Field and MD Parameters. In this investigation, the structures and properties of LMs of amphiphilic bistable [2]rotaxanes were simulated in the presence of a water subphase, using MD with a full atomistic force field. Here we employed the Dreiding force field,[70] which is a generic force field well tested in our previous study for

(33) Heath, J. R.; Ratner, M. A. *Phys. Today* **2003**, *56*, 43−49.
(34) Balzani, V.; Gomez-Lopez, M.; Stoddart, J. F. *Acc. Chem. Res.* **1998**, *31*, 405−414.
(35) Balzani, V.; Credi, A.; Raymo, F. M.; Stoddart, J. F. *Angew. Chem., Int. Ed.* **2000**, *39*, 3349−3391.
(36) Chia, S. Y.; Cao, J. G.; Stoddart, J. F.; Zink, J. I. *Angew. Chem., Int. Ed.* **2001**, *40*, 2447−2451.
(37) Belohradsky, M.; Elizarov, A. M.; Stoddart, J. F. *Collect. Czech. Chem. Commun.* **2002**, *67*, 1719−1728.
(38) Hernandez, R.; Tseng, H. R.; Wong, J. W.; Stoddart, J. F.; Zink, J. I. *J. Am. Chem. Soc.* **2004**, *126*, 3370−3371.
(39) Badjic, J. D.; Balzani, V.; Credi, A.; Silvi, S.; Stoddart, J. F. *Science* **2004**, *303*, 1845−1849.
(40) Tseng, H. R.; Vignon, S. A.; Celestre, P. C.; Perkins, J.; Jeppesen, J. O.; Di Fabio, A.; Ballardini, R.; Gandolfi, M. T.; Venturi, M.; Balzani, V.; Stoddart, J. F. *Chem. Eur. J.* **2004**, *10*, 155−172.
(41) Livoreil, A.; Dietrichbuchecker, C. O.; Sauvage, J. P. *J. Am. Chem. Soc.* **1994**, *116*, 9399−9400.
(42) Flood, A. H.; Peters, A. J.; Vignon, S. A.; Steuerman, D. W.; Tseng, H.-R.; Kang, S.; Heath, J. R.; Stoddart, J. F. *Chem. Eur. J.* **2004**, *24*, 6558−6561.
(43) Steuerman, D. W.; Tseng, H.-R.; Peters, A. J.; Flood, A. H.; Jeppesen, J. O.; Nielsen, K. A.; Stoddart, J. F.; Heath, J. R. *Angew Chem., Int. Ed.* **2004**, *43*, 6486−6491.
(44) Lee, I. C.; Frank, C. W.; Yamamoto, T.; Tseng, H.-R.; Flood, A. H.; Stoddart, J. F.; Jeppesen, J. O. *Langmuir* **2004**, *20*, 5809−5828.
(45) Tseng, H. R.; Wu, D. M.; Fang, N. X. L.; Zhang, X.; Stoddart, J. F. *ChemPhysChem* **2004**, *5*, 111−116.
(46) Raehm, L.; Kern, J. M.; Sauvage, J. P.; Hamann, C.; Palacin, S.; Bourgoin, J. P. *Chem. Eur. J.* **2002**, *8*, 2153-2162.
(47) Stoddart, J. F. *Chem. Aust.* **1992**, *59*, 576−577 and 581.
(48) Preece, J. A.; Stoddart, J. F. *Nanobiology* **1994**, *3*, 149−166.
(49) GomezLopez, M.; Preece, J. A.; Stoddart, J. F. *Nanotechnology* **1996**, *7*, 183−192.
(50) Pease, A. R.; Jeppesen, J. O.; Stoddart, J. F.; Luo, Y.; Collier, C. P.; Heath, J. R. *Acc. Chem. Res.* **2001**, *34*, 433−444.
(51) Colasson, B. X.; Dietrich-Buchecker, C.; Jimenez-Molero, M. C.; Sauvage, J. P. *J. Phys. Org. Chem.* **2002**, *15*, 476−483.
(52) Lehn, J.-M. *Angew. Chem., Int. Ed. Engl.* **1988**, *27*, 89−112.
(53) Lindsey, J. S. *New J. Chem.* **1991**, *15*, 153−180.
(54) Philp, D.; Stoddart, J. F. *Synlett* **1991**, 445−458.
(55) Lawrence, D. S.; Jiang, T.; Levett, M. *Chem. Rev.* **1995**, *95*, 2229−2260.
(56) Philp, D.; Stoddart, J. F. *Angew. Chem., Int. Ed. Engl.* **1996**, *35*, 1155−1196.
(57) Seeman, N. C. *Angew. Chem., Int. Ed.* **1998**, *37*, 3220−3238.
(58) Westhof, E.; Leontis, N. *Angew. Chem., Int. Ed.* **2000**, *39*, 1587−1591.
(59) Niemeyer, C. M.; Adler, M. *Angew. Chem., Int. Ed.* **2002**, *41*, 3779−3783.
(60) Kim, K.; Jeon, W. S.; Kang, J. K.; Lee, J. W.; Jon, S. Y.; Kim, T. *Angew. Chem., Int. Ed.* **2003**, *42*, 2293−2296.
(61) Long, B.; Nikitin, K.; Fitzmaurice, D. *J. Am. Chem. Soc.* **2003**, *125*, 15490−15498.
(62) Azehara, H.; Mizutani, W.; Suzuki, Y.; Ishida, T.; Nagawa, Y.; Tokumoto, H.; Hiratani, K. *Langmuir* **2003**, *19*, 2115−2123.
(63) Katz, E.; Sheeney-Haj-Ichia, L.; Willner, I. *Angew. Chem., Int. Ed.* **2004**, *43*, 3292−3300.
(64) Ahuja, R. C.; Caruso, P. L.; Mobius, D.; Philp, D.; Preece, J. A.; Ringsdorf, H.; Stoddart, J. F.; Wildburg, G. *Thin Solid Films* **1996**, *285*, 671−677.
(65) Amabilino, D. B.; Asakawa, M.; Ashton, P. R.; Ballardini, R.; Balzani, V.; Belohradsky, M.; Credi, A.; Higuchi, M.; Raymo, F. M.; Shimizu, T.; Stoddart, J. F.; Venturi, M.; Yase, K. *New J. Chem.* **1998**, *22*, 959−972.
(66) Asakawa, M.; Higuchi, M.; Mattersteig, G.; Nakamura, T.; Pease, A. R.; Raymo, F. M.; Shimizu, T.; Stoddart, J. F. *Adv. Mater.* **2000**, *12*, 1099−1107.
(67) Brown, C. L.; Jonas, U.; Preece, J. A.; Ringsdorf, H.; Seitz, M.; Stoddart, J. F. *Langmuir* **2000**, *16*, 1924−1930.
(68) Ulman, A. *An Introduction to Ultrathin Organic Films*; Academic Press: San Diego, 1991.
(69) Jang, S. S.; Jang, Y. H.; Kim, Y.-H.; Goddard, W. A., III; Flood, A. H.; Laursen, B. W.; Tseng, H.-R.; Stoddart, J. F.; Jeppesen, J. O.; Choi, J. W.; Steuerman, D. W.; DeIonno, E.; Heath, J. R. *J. Am. Chem. Soc.* **2005**, *127*, 1563−1575.
(70) Mayo, S. L.; Olafson, B. D.; Goddard, W. A., III. *J. Phys. Chem.* **1990**, *94*, 8897−8909.

[2]rotaxane SAMs on Au (111) surfaces[69,71] and for numerous other complex self-organized systems.[72,73] The F3C water model[74] was used to describe the interactions between water molecules. For the interactions between water and the rotaxanes, we used the standard geometric combination rules for Lennard-Jones potentials. The total potential energy is given as follows:

$$E_{\text{total}} = E_{\text{vdW}} + E_{\text{Q}} + E_{\text{bond}} + E_{\text{angle}} + E_{\text{torsion}} + E_{\text{inversion}} \quad (1)$$

where E_{vdW}, E_{Q}, E_{bond}, E_{angle}, E_{torsion}, and $E_{\text{inversion}}$ are the van der Waals, electrostatic, bond stretching, angle bending, torsion, and inversion components, respectively. The detailed force field parameters have been reported previously.[70,74]

The atomic charges on the rotaxanes were assigned using the charge equilibration (QEq) method,[75] and the atomic charges of the water molecules were taken from the F3C water model.[74] The particle−particle, particle−mesh Ewald (PPPM) method[76] was used for the long-range electrostatic interaction correction.

The simulations reported in this investigation were performed using the canonical ensemble (NVT) MD in which the Nose−Hoover thermostat[77,78] was used with a relaxation time of 0.1 ps. The equation of motion was integrated by the Verlet algorithm[79] with a time step of 1.0 fs. The MD software employed in this study was the large-scale atomic/molecular massively parallel simulator (LAMMPS)[80,81] code from Sandia National Laboratories which was modified to run our Dreiding force field and has been successfully used for our various studies.[69,72,73,82]

2.2. Model and MD Simulation. For our MD simulations we modified the spacer between the mpTTF unit and the hydrophilic stopper. The phenyl ring from the bistable rotaxane structure in Figure 1a was removed, as was the ethylene glycol linkers from the blocked rotaxanes in parts d and e of Figure 1.

To simulate a Langmuir monolayer computationally, it is convenient to use the two-monolayer arrangement shown in Figure 2b. As shown in our previous study on the surfactant-mediated air/water interface,[83] this symmetric configuration makes it possible to remove some mechanical unbalance caused by the asymmetry of a one-monolayer configuration, which may especially affect the surface tension. Another benefit is that we can obtain two independent samplings from one system. To determine the optimum configuration, first, we packed four rotaxanes with spacings suitable for hexagonal closest packing but in an orthorhombic simulation box with periodic boundary conditions applied for all three spatial directions, as shown in Figure 2a. To investigate the effect of the available packing area on the structures and properties of the LMs, we prepared monolayers with various surface areas, ranging from 124.71 to 312.64 Å^2/molecule, by setting the value of unit cell parameters $a = b$ (Figure 2a) to various values between 12 and 19 Å. We then minimized the energy to relax this rotaxane monolayer within the dimensions of the fixed simulation box. Next we placed this rotaxane monolayer on top of water with the same cell parameters and energy-minimized to obtain a good interaction between each rotaxane monolayer and the water subphase. For the air phase in this study, we used a vacuum as in our previous study[73] as well as studies by other groups[84−95] because the current simulated system with ∼70 000 Å^3 of air phase allows just one or two gas molecules under the atmospheric condition at 300 K.

After this initial configuration was prepared, we equilibrated the system (Figure 2b) by carrying out NVT MD simulations at 300 K for 1 ns. After this equilibration, we carried out another 4 ns of MD simulation for each co-conformation for each fixed packing area to obtain the data for our analyses. Table 1 summarizes the composition of the simulations and the dimension of each simulation box. Figure 3 shows the snapshots of equilibrated monolayer superstructures of each simulation box.

3. Results and Discussion

3.1. Electron Density Profiles. In this investigation, we calculated the electron density profiles for the simulated LMs on a water subphase. Since this electron density profile has been determined experimentally by X-ray reflectivity measurements, it is possible to compare our prediction directly with the experimental observations. For this analysis, we sliced the simulated system into 1.5 Å thick slabs parallel to the *xy* plane (and water surface) and calculated the electron density in each slab using eq 2,

$$\rho(z)/\rho_0 = \frac{1}{V_{\text{slab}}} \sum_{i(z)} (n_i + \delta_i) \quad (2)$$

where $\rho(z)$ and ρ_0 are the electron density of each slab at z and the electron density of the bulk water phase, respectively, and V_{slab} is the volume of the slab. n_i is the number of electrons belonging to atom i in the slab at z, and δ_i is the atomic partial charge of atom i calculated by the QEq method.[75] In Figure 4a,b, we display the electron density profiles of the simulated LMs for both co-conformations of the rotaxane, CBPQT^{4+}@mpTTF (Figure 1b) and CBPQT^{4+}@DNP (Figure 1c), with packing areas of 194.86 Å^2/molecule (the system of 15×15). We found that the electron density profile calculated for the simulated LM (thick solid line with solid squares in Figure 4a,b) agrees very well with the experimental profiles[96] (thick gray dashed line in Figure 4a,b) obtained from the LM with a similar packing area (ca. 180 Å^2/molecule).[97] We believe that this agreement of our simulation with the experimental observation supports the validity of our simulated model.

(71) Jang, Y. H.; Jang, S. S.; Goddard, W. A., III. *J. Am. Chem. Soc.* **2005**, *127*, 4959−4964.
(72) Jang, S. S.; Molinero, V.; Cagin, T.; Goddard, W. A., III. *J. Phys. Chem. B* **2004**, *108*, 3149−3157.
(73) Jang, S. S.; Lin, S.-T.; Maiti, P. K.; Blanco, M.; Goddard, W. A., III; Shuler, P.; Tang, Y. *J. Phys. Chem. B* **2004**, *108*, 12130−12140.
(74) Levitt, M.; Hirshberg, M.; Sharon, R.; Laidig, K. E.; Daggett, V. *J. Phys. Chem. B* **1997**, *101*, 5051.
(75) Rappe, A. K.; Goddard, W. A., III. *J. Phys. Chem.* **1991**, *95*, 3358−3363.
(76) Hockney, R. W.; Eastwood, J. W. *Computer Simulation Using Particles*; McGraw-Hill International Book Co.: New York, 1981.
(77) Nose, S. *J. Chem. Phys.* **1984**, *81*, 511−519.
(78) Hoover, W. G. *Phys. Rev. A* **1985**, *31*, 1695−1697.
(79) Verlet, L. *Phys. Rev.* **1967**, *159*, 98−103.
(80) Plimpton, S. J. *J. Comput. Phys.* **1995**, *117*, 1−19.
(81) Plimpton, S. J.; Pollock, R.; Stevens, M. *Eighth SIAM Conference on Parallel Processing for Scientific Computing*: Minneapolis, MN, March 14−17, 1997; SIAM: Philadelphia, PA, 1997.
(82) Jang, S. S.; Lin, S.-T.; Cagin, T.; Molinero, V.; Goddard, W. A., III. *J. Phys. Chem. B* **2005**, *109*, 10154−10167.
(83) Jang, S. S.; Lin, S.-T.; Maiti, P. K.; Blanco, M.; Goddard, W. A., III; Shuler, P.; Tang, Y. C. *J. Phys. Chem. B* **2004**, *108*, 12130−12140.
(84) Freeman, K. S. C.; McDonald, I. R. *Mol. Phys.* **1973**, *26*, 529−537.
(85) Liu, K. S. *J. Chem. Phys.* **1974**, *60*, 4226.
(86) Rao, M.; Levesque, D. *J. Chem. Phys.* **1976**, *65*, 3233.
(87) Miyazaki, J.; Barker, J. A.; Pound, G. M. *J. Chem. Phys.* **1976**, *64*, 3364.
(88) Rao, M.; Berne, B. J. *Mol. Phys.* **1979**, *37*, 455.
(89) Lee, C. Y.; Scott, H. L. *J. Chem. Phys.* **1980**, *73*, 4591.
(90) Townsend, R. M.; Gryko, J.; Rice, S. A. *J. Chem. Phys.* **1985**, *82*, 4391.
(91) Wilson, M. A.; Pohorille, A.; Pratt, L. R. *J. Phys. Chem.* **1987**, *91*, 4873.
(92) Brodskaya, E. N.; Rusanov, A. I. *Mol. Phys.* **1987**, *62*, 251.
(93) Matsumoto, M.; Kataoka, J. *J. Chem. Phys.* **1988**, *88*, 3233.
(94) Benjamin, I. *J. Chem. Phys.* **1991**, *94*, 662.
(95) Harris, J. G. *J. Phys. Chem.* **1992**, *96*, 5077.
(96) Norgaard, K.; Jeppesen, J. O.; Laursen, B. W.; Simonsen, J. B.; Weygand, M. J.; Kjaer, K.; Stoddart, J. F.; Bjornholm, T. *J. Phys. Chem. B* **2005**, *109*, 1063−1066.
(97) A monolayer of the amphiphilic [2]rotaxane (Figure 1a) was spread from a $CHCl_3$ solution (∼0.5−1.0 mg/mL) onto a purified H_2O surface in an LB trough. The subphase was 18.2 M cm (Milli-Q) H_2O. The $CHCl_3$ was passed through a column of basic alumina prior to use, to remove traces of HCl. The subphase was thermostated to 20 °C, and the monolayers were compressed at a (constant) rate of 5 A^2/molecule per minute while the surface pressure was monitored.

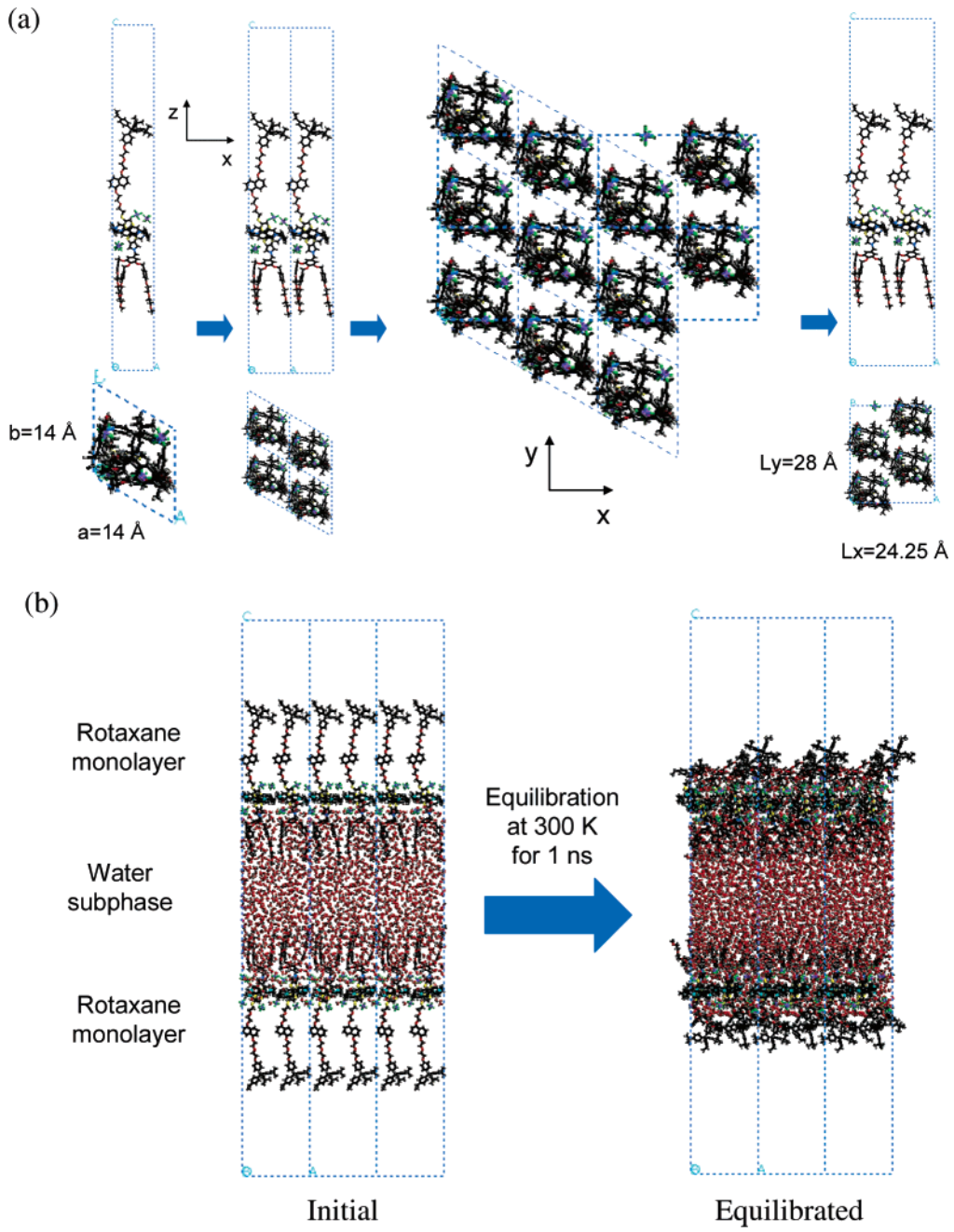

Figure 2. (a) Preparation of initial configuration of rotaxane monolayer. A hexagonal closed packing mode is retained in an orthorhombic simulation box consisting of four independent rotaxane molecules. (b) System configuration simulated in this study. Presented is the case of 169.74 Å^2/molecule (14 × 14).

Table 1. Simulation Results on the Doubled Langmuir Monolayers in Which Each Systems Has Two Monolayers with Four Rotaxane Molecules Packed Hexagonally, as Shown in Figure 2

system	$a = b$ (Å)	L_x (Å)	L_y (Å)	L_z (Å)	no. of water molecules	area/molecule (Å^2)
12 × 12	12	20.78	24.0	200	800	124.71
13 × 13	13	22.52	26.0		1010	146.36
14 × 14	14	24.25	28.0		1246	169.74
15 × 15	15	25.98	30.0		1498	194.86
16 × 16	16	27.71	32.0		1854	221.70
19 × 19	19	32.91	38.0		2514	312.64

A benefit of the *simulated* electron density profiles is that the overall electron density profile can be decomposed into the contributions from each component, as shown in Figure 4c, and we thereby can elucidate how the amphiphilic bistable [2]-rotaxane molecules self-organize in the LM at a given packing area at the air−water interface. In this computational study, we have defined the thickness of the LM as the distance between the two heights where the electron density of rotaxane monolayer is 10% of its maximum value (Figure 4c). Figure 5 shows the change of electron density profile for both co-conformations as a function of the packing area. From the simulations, we have found that, although the peak position in the electron density profile is different between the two co-conformations, this difference disappears with increasing area per molecule. The overall electron density profiles are very similar for both co-conformations over the whole range of packing areas characterized in the simulations. Hence, one co-conformation may not be so distinguishable from the other one when comparing the overall electron density profiles obtained from

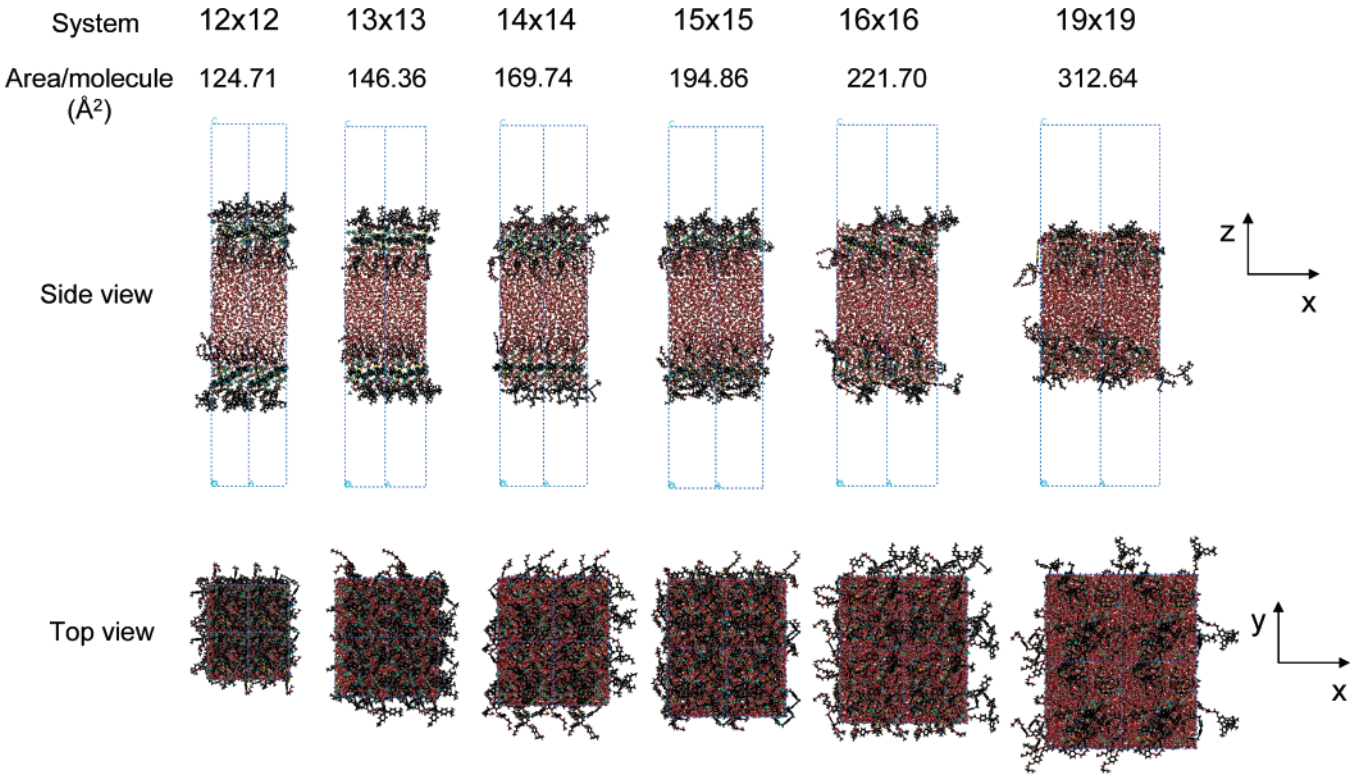

Figure 3. Snapshots of the equilibrated systems with various area per molecule summarized in Table 1 for the cases of $CBPQT^{4+}$@mpTTF. The cases of $CBPQT^{4+}$@DNP have similar feature in such snapshots.

Table 2. Structural Information of Amphiphilic Bistable [2]Rotaxane Langmuir Monolayers on Water

		system					
		12 × 12	13 × 13	14 × 14	15 × 15	16 × 16	19 × 19
area/molecule (Å²)		124.71	146.36	169.74	194.86	221.70	312.64
LM thickness (Å)	@mpTTF	44.2	42.5	41.1	40.4	36.8	36.6
	@DNP	43.3	41.0	42.3	40.5	37.1	36.7
Δz (Å) (DNP − mpTTF)	@mpTTF	10.5	9.0	8.5	8.0	7.5	7.5
	@DNP	9.0	8.0	7.5	6.0	5.5	4.5
position of $CBPQT^{4+}$ (Å)	@mpTTF	39.0	36.0	34.5	34.5	34.5	32.5
	@DNP	43.5	40.5	38.0	37.0	36.5	34.5
water level (Å)	@mpTTF	47.5	46.0	44.5	42.5	42.0	41.5
	@DNP	55.1	50.1	37.5	46.1	45.1	43.1

the X-ray reflectivity experiments. In this simulation study, however, by focusing on the contributions of each component, such as the mpTTF and DNP units and the $CBPQT^{4+}$ ring, the similar overall profiles can be resolved and only then can we characterize the structural differences between the two co-conformations, $CBPQT^{4+}$@mpTTF and $CBPQT^{4+}$@DNP. Table 2 summarizes all the information from the LM on water for both co-conformations at different packing areas.

It is obvious from an inspection of the data in Table 2 that the thickness of the LM decreases with increasing area per molecule, indicating that the rotaxane molecules, in the moderately compressed monolayers, are tilted down onto the water surface. Similar changes of the LM electron density profiles as a function of the area per molecule were observed experimentally by X-ray measurements[96] on LMs (Figure 1a) at 180, 265, and 470 Å². A point of interest here is that the LM thicknesses are very similar, irrespective of the co-conformation. Similarly, we observed the same feature in a related study[69] on SAMs of bistable [2]rotaxanes on Au (111) surfaces. Therefore, we confirm again that shuttling of the $CBPQT^{4+}$ ring between mpTTF and DNP units is not necessarily accompanied by significant dimensional changes of the monolayers' superstructures, a finding that may be important in the fabrication and operation of solid-state devices.

Next, we investigated the change in the relative positions of mpTTF and DNP along the *z*-axis direction within the LM as a function of packing area. From Table 2, it is noticeable that the difference (Δz) between the DNP and mpTTF units decreases for both co-conformations as the area per molecule increases, an observation which is consistent with the decreasing trend in the LM thickness. A somewhat interesting feature is, however, the fact that the Δz for the $CBPQT^{4+}$@mpTTF co-conformation is larger than that for the $CBPQT^{4+}$@DNP one, a divergence which becomes more distinguished as the packing area decreases, so that the difference ($\Delta Z_{CBPQT@mpTTF} - \Delta Z_{CBPQT@DNP}$) is increased. We think that such difference is attributed to the different solvation of the LMs in the two co-conformations.

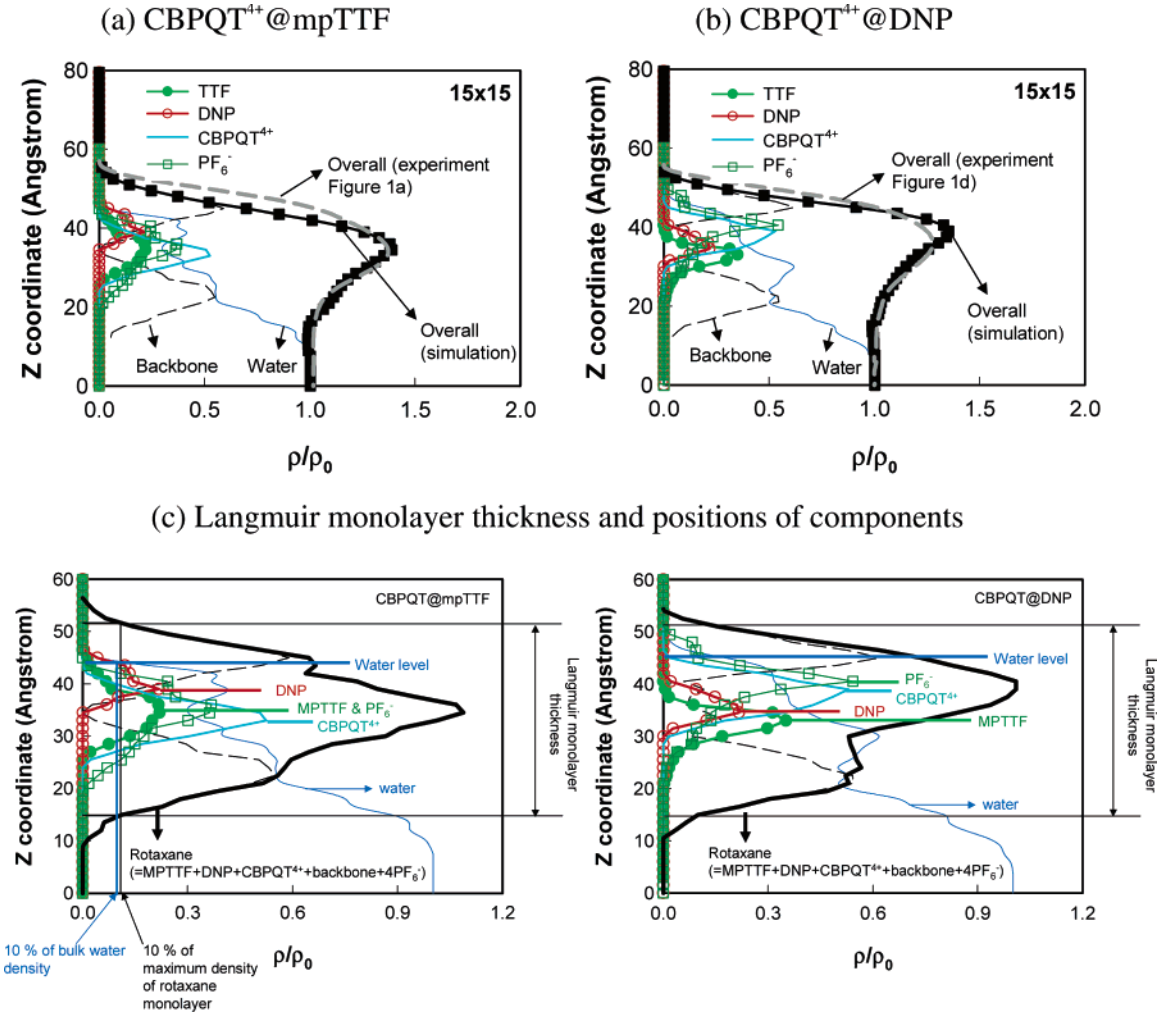

Figure 4. Normalized electron density profiles calculated from our simulations for $CBPQT^{4+}$@mpTTF and $CBPQT^{4+}$@DNP with 194.86 Å^2/molecule (15 × 15) packing. Here, the values were normalized by the electron density of bulk water phase (ρ_0), so that the water phase has the value of 1.0.

The positions of the $CBPQT^{4+}$ ring and the PF_6^- counterions were analyzed in a similar manner. It is observed (Figures 4 and 5) during 4 ns MD simulations that the $CBPQT^{4+}$ rings, together with the PF_6^- counterions, stay on the mpTTF and on the DNP for each co-conformation, $CBPQT^{4+}$@mpTTF and $CBPQT^{4+}$@DNP, respectively. This information on the positions of the counterion (PF_6^-) is especially important because the counterions sustain this kind of supramolecular self-assembled structure by screening the repulsive charge−charge interaction between the charged entities through pairing with the $CBPQT^{4+}$ ring. Otherwise, the electrostatic repulsion would break the self-assembled feature. In this context, we may raise a related question about the behavior of the counterion during the shuttling movement of the $CBPQT^{4+}$ ring, which we reasonably expect should affect the kinetics of the transition between the stable state and the metastable one. We have to leave this question for future study since in this study we focus only on the structures and properties of the two states. The DNP unit is situated at the upper site in the molecular structure of the [2]rotaxane (Figure 1a,b), and so the *z* coordinate of the $CBPQT^{4+}$ ring is higher in the $CBPQT^{4+}$@DNP co-conformation than it is in the $CBPQT^{4+}$@mpTTF, a property which is reflected by the rotaxane's component peak positions in the overall electron density profile. However, as the area per molecule increases, the *z* coordinate of the $CBPQT^{4+}$ ring becomes similar for both co-conformations on account of the molecules' tilting and folding behavior (see Table 2). This observation is also consistent with the change in the LM thickness as a function of packing area.

Other important factors are the water level and the monolayer's degree of hydration, both of which are related to the solvation of the LM. In this study, we have defined the water level as the *z* coordinate of the position where the electron density of water is 10% of bulk water density (Figure 4c). The amphiphilic bistable [2]rotaxane was designed (Figure 1) to bear a bulky hydrophobic tetraarylmethane stopper at one end of the dumbbell and, at the other end, a bulky hydrophilic dendritic group. Thus, these constituents impart surfactant-like characteristics to the [2]rotaxane. By partitioning a whole rotaxane molecule into four important parts—the hydrophilic dendritic endgroup (Dend), mpTTF, DNP, and the hydrophobic tetraarylmethane endgroup (TAM) (Figure 6a,b)—we can appreciate that the shuttling of the $CBPQT^{4+}$ ring between the mpTTF and the DNP units causes a change in the hydrophilic/hydrophobic sequence in the [2]rotaxane molecule. In other words, for the $CBPQT^{4+}$@mpTTF co-conformation, the sequence of the component parts defines a bipolar arrangement (**hydrophilic Dend endgroup/hydrophilic $CBPQT^{4+}$-on-mpTTF**/*hydrophobic DNP/hydrophobic TAM endgroup*), whereas the hydrophilic part and the hydrophobic part are of an alternating

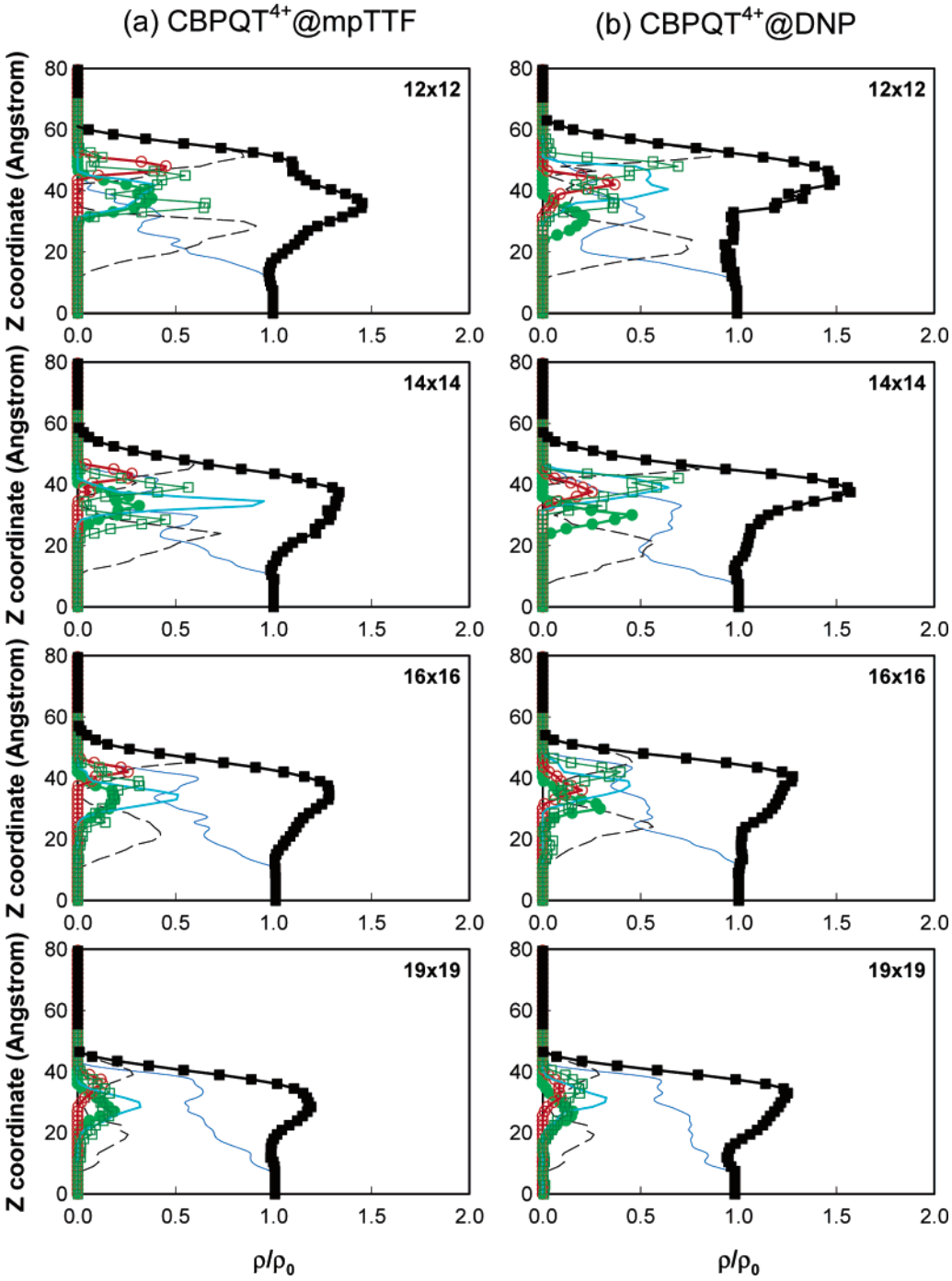

Figure 5. Evolution of electron density profiles as a function of area per molecule. The legend is the same as in Figure 4.

sequence for the CBPQT^{4+}@DNP (**hydrophilic Dend end-group**/*hydrophobic mpTTF*/**hydrophilic CBPQT^{4+}-on-DNP**/*hydrophobic TAM endgroup*). Hence, to solvate the hydrophilic CBPQT^{4+} ring and its counterions, therefore, the water has to rise up to its position through the LM. We found (Table 2) that the water level for the CBPQT^{4+}@DNP co-conformation is higher by ∼10 Å than for the CBPQT^{4+}@mpTTF one at the packing area of 124.71 Å^2/molecule, but such differences in the water level become smaller as the area per molecule increases, a phenomenon which is also a consequence of the molecular tilt of the rotaxane.

We believe that these results also explain why the Δ*z* (DNP-mpTTF) is smaller (Table 2) for the CBPQT^{4+}@DNP co-conformation than for the CBPQT^{4+}@mpTTF one. First, for the CBPQT^{4+}@mpTTF co-conformation with the bipolar sequence, the rotaxane molecules behave like a surfactant since the **hydrophilic dendritic group** and the **hydrophilic CBPQT^{4+}-on-mpTTF** tend to be solvated by water and *the hydrophobic parts* are not. By contrast, for the CBPQT^{4+}@DNP co-conformation with the alternating sequence, the **hydrophilic dendritic group** and the **hydrophilic CBPQT^{4+}-on-DNP** are separated by *hydrophobic mpTTF*, so that the DNP unit in a rotaxane tends to tilt down on the water surface to maximize the favorable contact between the **hydrophilic CBPQT^{4+}-on-DNP** and **water**. We believe that this explanation is the reason that the Δ*z* (DNP-mpTTF) for CBPQT^{4+}@DNP is smaller than

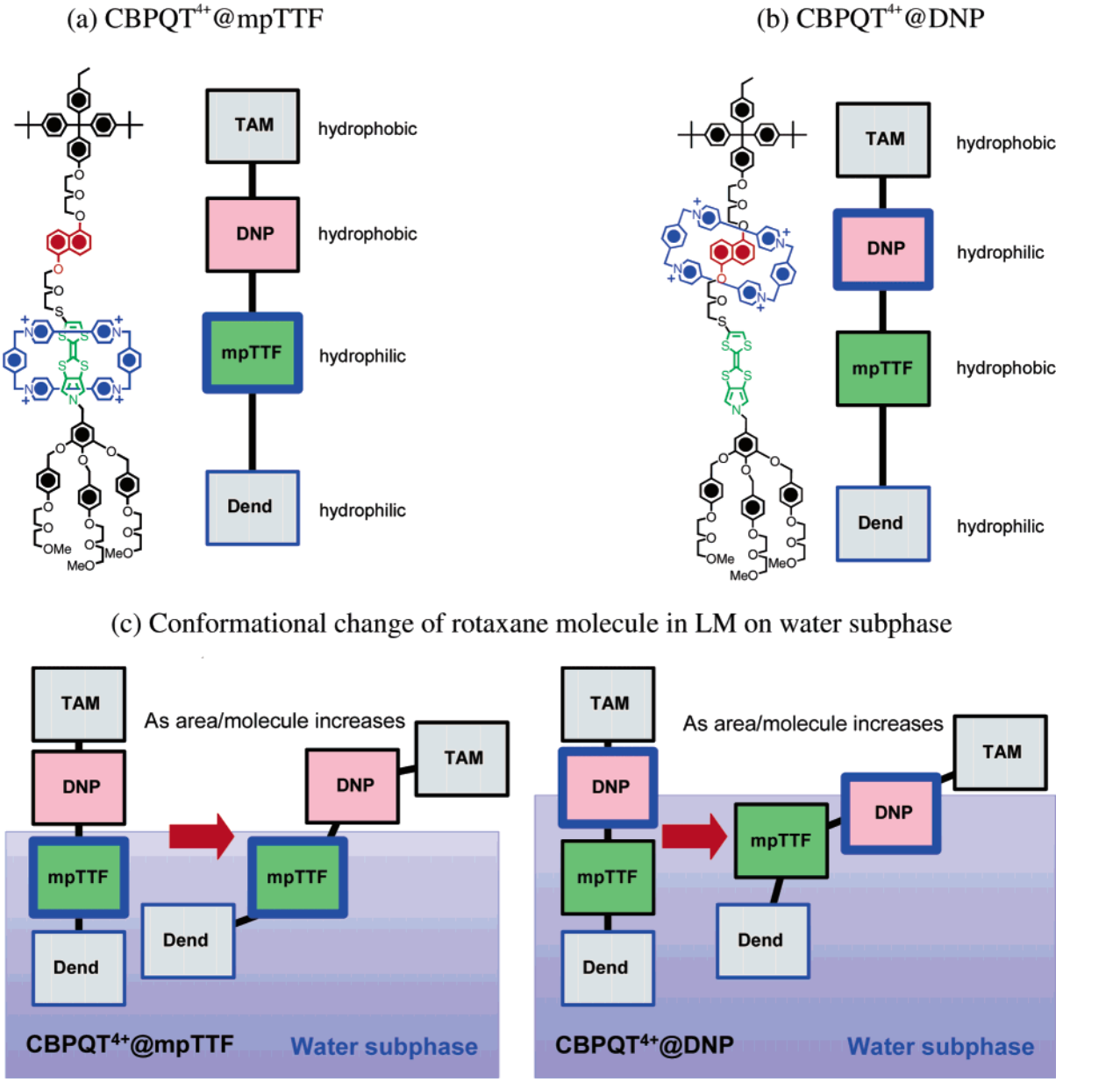

Figure 6. Schematic presentation of amphiphilic bistable [2]rotaxane with unit hydrophilicity/hydrophobicity.

that for CBPQT^{4+}@mpTTF, as summarized in Figure 6c. These structural models of the loosely compressed LMs in Figure 6 agree well with qualitative models that have been suggested previously based on LM isotherm[44] and surface X-ray[96] studies.

The degree of hydration was also calculated by counting the number of water molecules in the rotaxane LM above the *z* coordinate, where the water electron density is less than that of bulk water. The number of water molecules increases (Table 3) as the packing area increases for both co-conformations, demonstrating that larger packing area per molecule densities provide more space within the LM to accommodate more water molecules in order to solvate the hydrophilic CBPQT^{4+} ring and its counterions. This result is also in good agreement with the experimental observations. Another point of note is that, at the same packing area per molecule, the number of water molecules is almost the same for both co-conformations. From this observation, the degree of hydration at a given packing area seems to be dominated by the hydrophilic/ionic components, namely the CBPQT^{4+} ring and its counterions.

Table 3. Numbers of Water Molecules per Rotaxane Molecule within Each Langmuir Monolayer on a Water Subphase

system	area/molecule (Å^2)	no. of water molecules/rotaxane[a]	
		CBPQT^{4+}@mpTTF	CBPQT^{4+}@DNP
12 × 12	124.71	11.26	11.27
13 × 13	146.36	21.32	22.26
14 × 14	169.74	26.94	27.46
15 × 15	194.86	35.68	35.60
16 × 16	221.70	37.00	36.96
19 × 19	312.64	60.46	60.69

[a] The number of water molecules in each rotaxane LM was counted from where the water electron density is less than that of the bulk water phase.

3.2. Tilt Angles for the Rotaxane. The typical equilibrated conformations (Figures 3 and 7) of the rotaxane in the LMs reveal that, since the rotaxane's backbone is flexible, it can adopt an enormous variety of conformations, and so there seems to be no unambiguous way to define molecular tilt angle. Thus, to evaluate the whole molecular tilt of the rotaxane in the LM quantitatively, we define (Figure 8a) the molecular tilt angle as

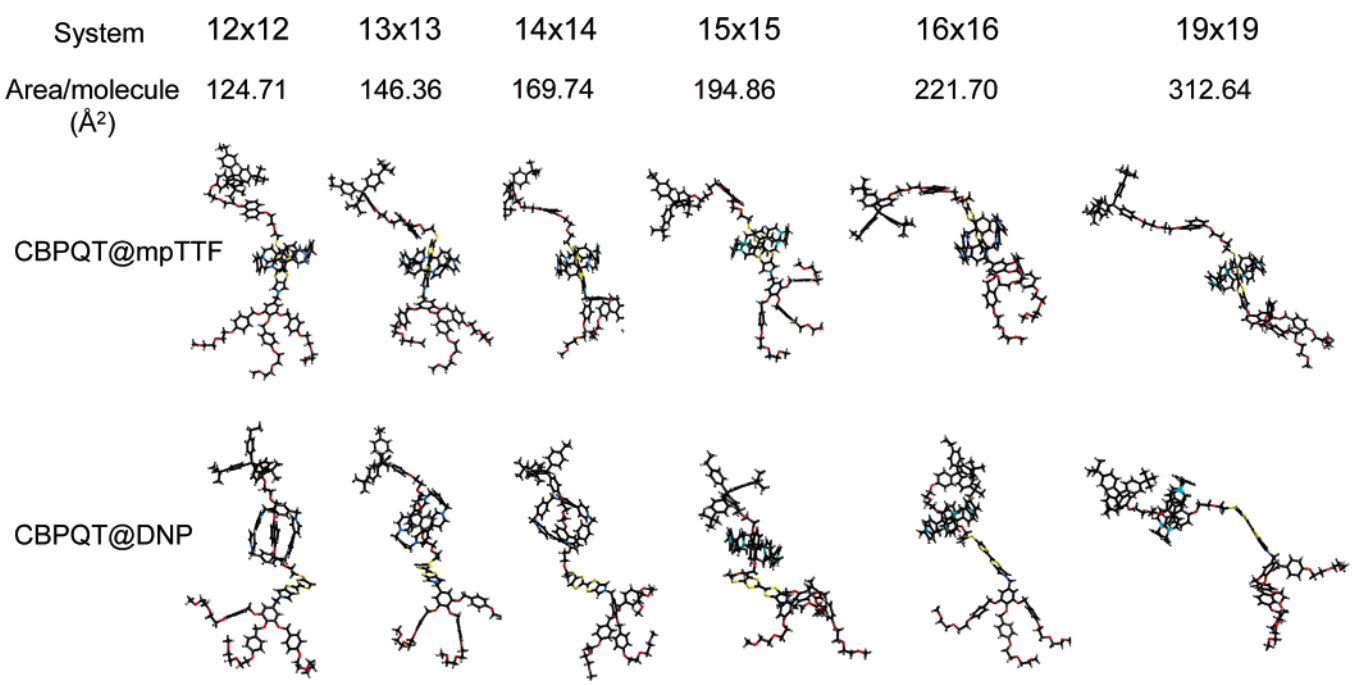

Figure 7. Typical conformations of rotaxane from the equilibrated Langmuir monolayer systems with the corresponding area per molecule.

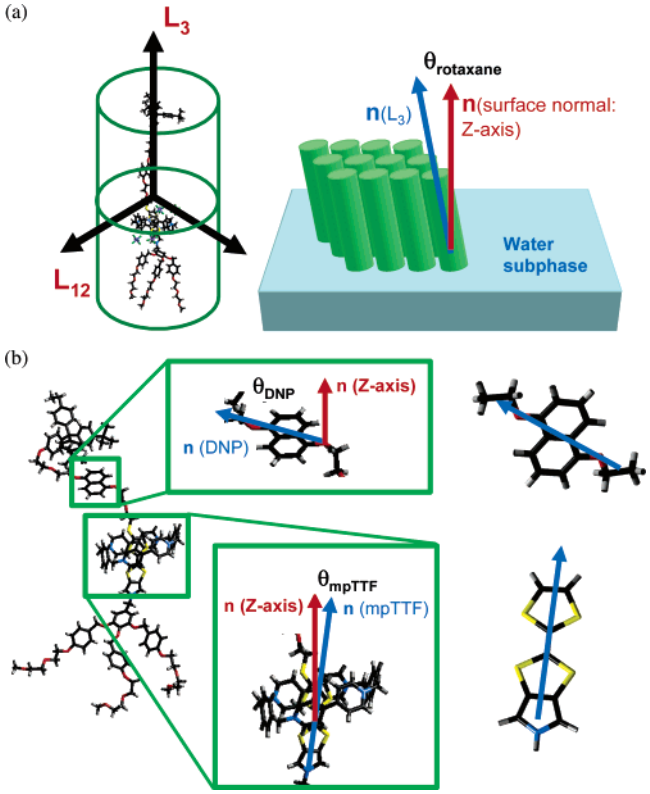

Figure 8. Tilt of (a) the whole rotaxane molecule and (b) the DNP and mpTTF moieties. L_3 denotes the longest principal axis of the moment of inertia, and $L_{12} = (L_1 + L_2)/2$.

the angle between the surface normal and the longest principal axis of moment of inertia. From Figure 9a, we can see that the CBPQT^{4+}@mpTTF and the CBPQT^{4+}@DNP co-conformations show almost the same change in the molecular tilt as a function of the packing area—first, the tilt angle gets smaller with decreasing area per molecule, and second, the magnitude of the tilt angle is practically the same for both co-conformations at the same packing area. Another interesting point, illustrated in Figure 9a, is that the molecular tilt angle decreases significantly in the range from ~200 to ~140 Å^2/molecule as the LM is compressed. We suspect that such a big change in tilt angle is significant and that it is related to the structural transition of LM from **the liquid expanded phase** to **the liquid condensed phase**. This hypothesis is also consistent with the experimental isotherms for rotaxanes in Figure 1a−c, where phase transitions are observed at mean molecular areas close to 160 Å^2, corresponding to the 14 × 14 system.

In this investigation, we also analyzed the conformation of the rotaxane by introducing two unit tilt angles as a means of visualizing and registering how the orientations of the mpTTF (the angle between the surface normal (*z*-axis) and the central carbon−carbon bond vector of mpTTF) and the DNP (the angle between the surface normal and the oxygen−oxygen vector of DNP) units change (Figure 8b) as the monolayer is compressed. The behavior of these unit tilt angles is found to be more complicated (Figure 9b) than that for the entire rotaxane. We have found that, for both co-conformations, the unit encircled by the CBPQT^{4+} ring has a small tilt angle, while the other unit has a significantly larger tilt angle. Interestingly, this difference in the unit tilt angles between mpTTF and DNP units decreases from 90° to 40° for the CBPQT^{4+}@mpTTF co-conformation, and from 70° to 5° for the CBPQT^{4+}@DNP co-conformation, as the area per molecule increases. These findings suggest that the CBPQT^{4+} ring places constraints on the packing arrangements that are accommodated by significant conformational folding of the remaining part of the rotaxane's backbone. From these unit tilt angles, we see that the amphiphilic rotaxane molecule adopts (Figure 7) a highly folded conformation, even at the small area per molecule. Another feature of note in Figure 9b is that, at the same packing area, such internal differences in unit tilt angles are smaller for the CBPQT^{4+}@DNP than for the CBPQT^{4+}@mpTTF. From these results, we may infer two points. First, although we do not see the actual shuttling motion of the CBPQT^{4+} ring between the mpTTF and DNP units during a 4 ns MD simulation, the shuttling should be somewhat easier

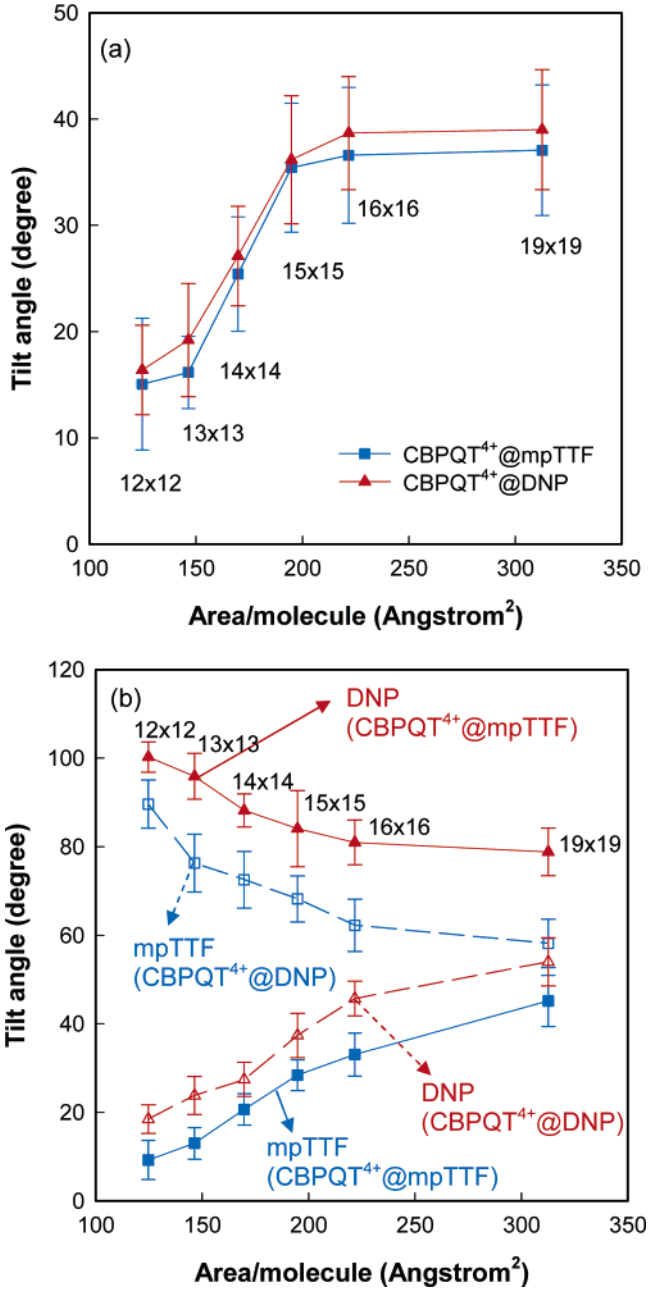

Figure 9. Change of tilt angle as a function of packing for (a) the whole rotaxane molecule and (b) the mpTTF and DNP units. Solid symbol denote the CBPQT^{4+}@mpTTF co-conformation and open symbols denote the CBPQT^{4+}@DNP co-conformation.

in the co-conformation CBPQT^{4+}@DNP than in the CBPQT^{4+}@mpTTF one because the unit tilt angle difference is smaller for the former co-conformation than for the latter. This observation means that, from the viewpoint of the rotaxane conformations, the switching-off action, corresponding to the movement of the CBPQT^{4+} ring from the DNP to the mpTTF station in LB-based molecular electronic devices, would be easier than the switching-on motion from the mpTTF to the DNP station, a process that requires considerably more conformational rearrangements. Second, the shuttling movement is also easier at a larger area per molecule (lower packing) than at a smaller one (higher packing) because the unit tilt angle difference is smaller at larger area per molecule than at smaller area per molecule.

3.3. Surface Pressure−Area Isotherms. Here, we report the theoretically predicted surface pressure−area isotherms for the amphiphilic bistable [2]rotaxanes in comparison with the experimental ones. The definition of surface pressure Π is

$$\Pi = \sigma_0 - \sigma \tag{3}$$

where σ_0 and σ are the surface tension of the air/water interface and of the air/rotaxane/water interfacial system (Langmuir monolayer), respectively. To calculate σ_0 and σ, using the following definition,

$$\sigma = \frac{1}{2}\int_0^L \mathrm{d}z\,[P_N(z) - P_T(z)] \tag{4}$$

we sliced the system into slabs with 1.5 Å thickness parallel to the *xy* (water) plane and calculated the normal and tangential components of the stress ($P_N(z)$ and $P_T(z)$) of each slab using the Kirkwood−Buff theory:[9898]

$$P_N(z) = \rho(z)k_BT - \frac{1}{V_{slab}}\left\langle \sum_{i,j} \frac{z_{ij}^2}{r_{ij}} \frac{\mathrm{d}u(r_{ij})}{\mathrm{d}r_{ij}} \right\rangle \tag{5}$$

$$P_T(z) = \rho(z)k_BT - \frac{1}{V_{slab}}\left\langle \sum_{i,j} \frac{x_{ij}^2 + y_{ij}^2}{2r_{ij}} \frac{\mathrm{d}u(r_{ij})}{\mathrm{d}r_{ij}} \right\rangle \tag{6}$$

where L is the dimension of the system in the *z*-axis direction, $\rho(z)$ and V_{slab} denote the density of the slab at z and the slab volume, respectively, and k_B and T are the Boltzmann constant and the absolute temperature, respectively. Angle brackets mean an ensemble average of all atoms located in the slab at z. r_{ij}, x_{ij}, y_{ij}, and z_{ij} are the distances between the atoms and their coordinate components, respectively, and $u(r_{ij})$ is the potential energy of the atomic pair i and j. Using this method with MD simulations in our previous study,[73] we could obtain the surface tension (interfacial tension) values for the interfacial systems such as air/decane (21.77 ± 2.31 dyn/cm; exp.[99] 23.20 dyn/cm), air/water (70.94 ± 2.25 dyn/cm; exp.[100,101] 71.71 dyn/cm), and decane/water (54.70 ± 3.62 dyn/cm; exp.[102] 51.72 dyn/cm).

The surface tension−area and surface pressure−area isotherms are presented in Figure 10. First, it is clearly observed (Figure 10a) that the surface tension (σ) increases with increasing area per molecule, so that the value of σ approaches the bare water surface tension (at 300 K, σ_0 = 70.94 dyn/cm in our simulation and 71.71 dyn/cm in the experiments) in the range of dilute surface concentrations. This behavior is a common one for the surface tension observed in simple amphiphilic molecules, such as surfactants. A point of interest here is that the surface tension of the CBPQT^{4+}@mpTTF co-conformation is smaller than that of the CBPQT^{4+}@DNP at the same area per molecule, an observation which is reflected directly in the surface pressure−area isotherm (Figure 10b) since these two isotherms are equivalent by definition as in eq 3. For

(98) Kirkwood, J. G.; Buff, F. P. *J. Chem. Phys.* **1949**, *17*, 338−343.
(99) Jasper, J. J. *J. Phys. Chem. Ref. Data* **1972**, *1*, 841−1009.
(100) Tsierkezos, N. G.; Molinou, I. E. *J. Chem. Eng. Data* **1998**, *43*, 989−993.
(101) Alvarez, E.; Rendo, R.; Sanjurjo, B.; Sanchez-Vilas, M.; Navaza, J. M. *J. Chem. Eng. Data* **1998**, *43*, 1027−1029.
(102) Zeppieri, S.; Rodriguez, J.; de Ramos, A. L. L. *J. Chem. Eng. Data* **2001**, *46*, 1086−1088.

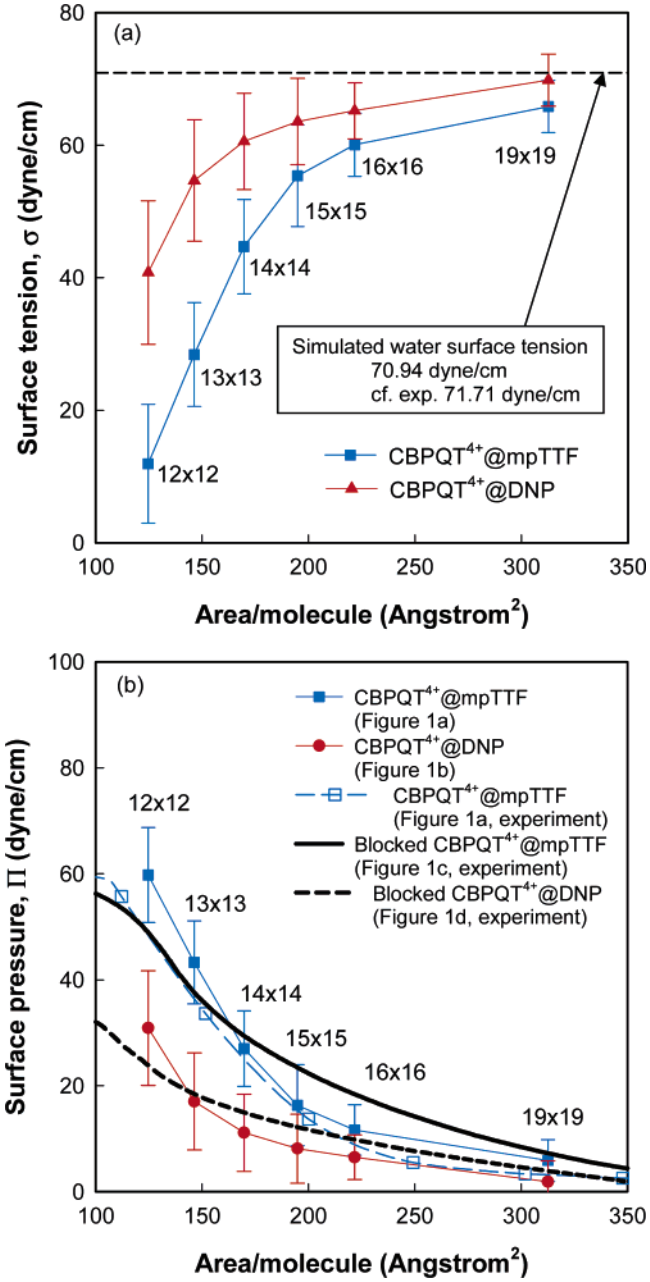

Figure 10. Change in surface tension and surface pressure as a function of area per molecule.

comparison, we present the experimental isotherms of the bistable rotaxane (Figure 1a) and two rotaxanes (Figure 1d,e) that serve as control systems wherein the CBPQT^{4+} ring is blocked sterically around the mpTTF or DNP unit, respectively. Because it is challenging to obtain/retain the CBPQT^{4+}@DNP co-conformation of bistable rotaxanes (Figure 1c) on pure water subphases without the use of oxidants, these blocked rotaxanes provide a model for the CBPQT^{4+}@DNP co-conformation. Comparison of the theoretically predicted surface pressure−area isotherms with the experimental results shows good qualitative agreement with experiment, namely that the CBPQT^{4+}@mpTTF co-conformation has larger surface pressures than the CBPQT^{4+}@DNP one at the same packing area. We consider this agreement as a general support of the validity of our simulations.

At this point, it is of interest to ask why the surface tension of the CBPQT^{4+}@mpTTF co-conformation is smaller than that of the CBPQT^{4+}@DNP one. A previous investigation[69] on a bistable [2]rotaxane self-assembled monolayer (SAM) on a Au (111) surface, in which similar molecular structures were used with the exception that the "parent" TTF unit was present rather than the mpTTF one, recorded similar results. The surface tension of the CBPQT^{4+}@TTF co-conformation is smaller than that of the CBPQT^{4+}@DNP one, a finding that can be explained by the difference in charge delocalization between these two co-conformations. Since the charge distribution is more efficiently delocalized in the CBPQT^{4+}@TTF co-conformation than in the CBPQT^{4+}@DNP one, on account of the more favorable intramolecular charge-transfer interactions, the former is less polar than the latter, a situation which affects the intermolecular interaction between individual rotaxane molecules, leading to a lower surface tension for the CBPQT^{4+}@TTF co-conformation.

In the present investigation, however, it should be noted that the LM consists of not only the rotaxane molecules but also water molecules from the subphase (as shown in Figures 2−5) and, furthermore, the LM's surface tension is produced as a consequence of these integrated structures, while the SAM system consisted of only rotaxanes chemisorbed on a Au surface without being mixed with water. Therefore, the surface tension of the LM must be understood in the context of how the rotaxane molecules incorporate water into the LM through the unit sequence of hydrophobic and hydrophilic units, as well as how individual rotaxane molecules interact with their neighboring rotaxane molecules in such a self-organized structure. Since the bipolar hydrophilic/hydrophobic unit sequence of the CBPQT^{4+}@mpTTF co-conformation has a greater surfactant-like character than the unit sequence associated with the CBPQT^{4+}@DNP co-conformation, it is also reasonable to infer that the former can reduce the water surface tension more efficiently than the latter. We expect, therefore, that at larger area per molecule values, the surfactant-like properties of the particular co-conformation will take a dominant role in determining the surface tension of rotaxane LMs on water, while the intermolecular interactions, depending on the charge delocalization within the rotaxane molecule, become important with smaller packing area per molecule densities and also when the number of water molecules in the rotaxane LM decreases.

4. Summary

Using a fully atomistic molecular dynamics simulation, we have predicted the structure and surface pressure−area isotherms of amphiphilic bistable [2]rotaxane Langmuir monolayer on water subphase.

From the simulated structures of the Langmuir monolayers, we have obtained the electron density profiles as a function of the monolayer packing area. They show good agreement with the experimental ones obtained from the X-ray reflectometry. We found that the LMs of the CBPQT^{4+}@mpTTF and CBPQT^{4+}@DNP co-conformations exhibit similar shapes for their overall electron density profiles. We have also found that the thickness of the LM decreases similarly for both co-conformations as the area per molecule increases, since the molecular tilt increases, as shown by the tilt angle analysis. Interestingly, the thickness of the LM was almost the same for both co-conformations at the same packing area.

Although both co-conformations of the LM systems have similar dimensions at the same packing area and similar in-plane expanding behavior with increasing area per molecule, we found distinct features by decomposing the overall electron density profile into the components' contributions—the distance in *z*-axis direction between the mpTTF and DNP (Δz) units, the position of $CBPQT^{4+}$ ring, and the water level. In contrast to the common feature for both co-conformations, namely that the Δz decreases with increasing area per molecule, the Δz for the $CBPQT^{4+}$@mpTTF co-conformation is larger than that for the $CBPQT^{4+}$@DNP one, a trend which becomes clearer as the area per molecule increases. This difference of Δz between the two co-conformations is rationalized by considering the hydrophilic/hydrophobic sequence of the units in the rotaxane molecule. Thus, the position of DNP in the $CBPQT^{4+}$@DNP co-conformation with the alternating sequence is lowered relative to the $CBPQT^{4+}$@mpTTF one in order to be favorably solvated by water. We also found that during 4 ns MD simulations, the $CBPQT^{4+}$ ring stays located on the electron-donating units—the mpTTF unit for $CBPQT^{4+}$@mpTTF and the DNP unit for CBPQT@DNP. Therefore, the position of the $CBPQT^{4+}$ ring is higher in the $CBPQT^{4+}$@DNP co-conformation than in the $CBPQT^{4+}$@mpTTF one since the position of the DNP unit is higher than that of mpTTF in the rotaxane backbone. However, this feature disappears as the molecular tilt increases with increasing area per molecule.

At the same area per molecule, the average molecular tilt seems to be the same for both co-conformations. Regardless of the configuration, the molecular tilt increases as the area per molecule increases. Specifically, it changes significantly over the range from $\sim$200 $Å^2$/molecule to $\sim$140 $Å^2$/molecule, where the LM seems to undergo a transition between the liquid expanded phase and the liquid condensed phase. We also analyzed the unit tilt—that is, the tilt of the mpTTF and DNP units relative to the surface normal—and found that the tilt angle of the unit with the $CBPQT^{4+}$ ring is smaller than that of the other unit that carries no ring, and this difference decreases with increasing area per molecule.

We have calculated the surface pressure−area isotherms for each configuration using the Kirkwood−Buff formula and found good agreement with the experimental ones: the $CBPQT^{4+}$@mpTTF co-conformation has smaller surface tension (larger surface pressure) than the $CBPQT^{4+}$@DNP one, at the same packing area, and this difference decreases with increasing area per molecule. We believe that these isotherms are affected by the unit sequence in rotaxane molecules, a structural feature which determines how the water is incorporated within the rotaxane LM.

Acknowledgment. The computational work was initiated with support by the National Science Foundation (NIRT, W.A.G.). The collaboration was supported by the Microelectronics Advanced Research Corporation (MARCO, J.F.S.) and its Focus Centers on Functional Engineered NanoArchitectonics (FENA) and Materials Structures and Devices, the Moletronics Program of the Defense Advanced Research Projects Agency (DARPA, J.F.S. and J.R.H.), the Center for Nanoscale Innovation for Defense (CNID, J.F.S.), and the MARCO Materials Structures and Devices Focus Center (J.R.H.). In addition, the facilities of the MSC (W.A.G.) were supported by ONR-DURIP, ARO-DURIP, IBM (SUR), and the Beckman Institute.

JA0531531